Lowland Technology International 2017; 19 (3): 219-230
International Association of Lowland Technology (IALT): ISSN 1344-9656
***Special Issue on: Kumamoto Earthquake & Disaster***

Research Paper

# Instability of residences founded on volcanic cohesive soils during the 2016 Kumamoto Earthquake

K. Yasuhara [1], H. Watanabe [2], K. Kobayashi [2], M. Yoshimi [3], Y. Arai [4], S. Hosoya [4] , M.S. Tajiri [5] and S. Murakami [6]

**ARTICLE INFORMATION**

***Article history:***

Received: 06 March, 2017
Received in revised form: 07 November, 2017
Accepted: 09 November, 2017
Publish on: 08 December, 2017

***Keywords:***

Damage
Residence with retaining wall
Kumamoto earthquake
Volcanic ash soil
Cyclic degradation
Excess pore water pressure
Lateral earth pressure

**ABSTRACT**

This paper is intended to describe that the nonlinearity of seismic response for soft deposits is associated with the cyclic degradation of strength and stiffness in shallow deposits of cohesive volcanic ash soils, which caused devastation to residences. Using the simplified methodologies proposed previously by the authors, which incorporate cyclic strength and stiffness degradation characteristics of saturated cohesive soils, prediction was conducted for residential settlement and lateral deformation of residences with retaining walls founded on and against a shallow layer of cohesive volcanic ash soils. A chart for construction management incorporating the results in terms of earthquake-induced settlement vs. lateral deformation-settlement relations predicted the use of the methodology described above. Results suggest that residences are likely to sustain severe damage when the normalized excess pore pressures generated during the earthquake extend to about 0.7. Results also show that damage to retaining walls was also associated with earthquake-induced strength degradation of backfill soils.

## 1. Introduction

A Mj6.5 earthquake event shook Kumamoto prefecture, Japan on April 14, 2016. Soon thereafter, on April 16, a Mj7.3 earthquake event struck Kumamoto and Oita prefectures. A recent investigation (AIST; Yoshimi et al., 2016) revealed that nonlinearity of the seismic response for deposits layered by volcanic ash cohesive soils and pumices caused devastating damage to residences of Mashiki-machi near Kumamoto city during the Kumamoto earthquake in 2016. According to those findings, the authors suspected that the nonlinearity of seismic response for soft deposits is associated with cyclic degradation of strength and stiffness in deposits of cohesive volcanic ash soils, causing extreme damage to residences. Using simplified methodologies (2001, 2004, 2017) proposed by the authors incorporating degradation characteristics of volcanic ash cohesive soils, the authors attempted to predict residential settlement and lateral deformation of cohesive volcanic ash soils that led to devastation damage in residential areas. Furthermore, some consideration was devoted to how retaining walls near residential houses were severely collapsed.

[1] Professor Emeritus, ICAS, Ibaraki University, Ibaraki 310-8512, JAPAN, kazuya.yasuhara.0927@vc.ibaraki.ac.jp
[2] Graduate student, School of Science & Technology, Ibaraki University, Ibaraki 316- 8511, JAPAN
[3] Professor, Dept. of Urban & Civil Engineering, Ibaraki University, Ibaraki 316-8511, JAPAN
[4] Senior Researcher, Geological Survey of Japan/AIST, Ibaraki 305-8560, Tsukuba, JAPAN
[5] Manager, Tajiri Corporation, Kumamoto, JAPAN
[6] Professor, Dept. of Civil Engineering, Fukuoka University, Fukuoka 814-0180, JAPAN
*Note:* Discussion on this paper is open until June 2018

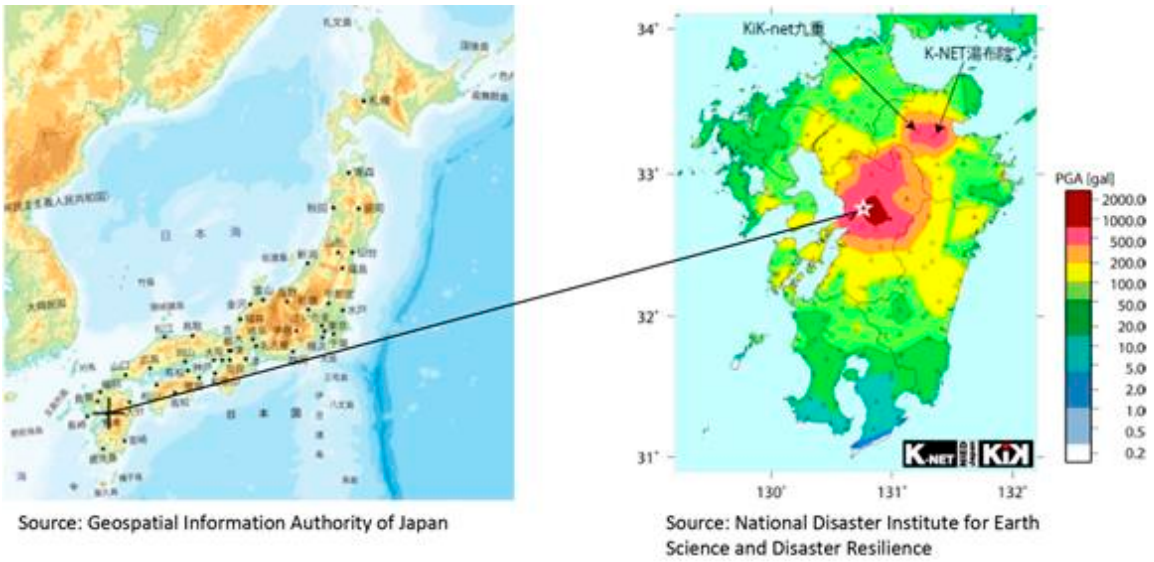


**Fig. 1.** Location of 2016 Kumamoto earthquake

Devastation included 64 lost fatalities and 8336 complete failures of residences was caused by the 2016 Kumamoto earthquake, which included a Mj6.5 earthquake foreshock on April 14, and a Mj7.3 main shock earthquake soon after on April 16, striking a Mj7.3 Kumamoto and Oita prefectures shown in Figure 1.

From geotechnical engineering points of view, damage was characterized as explained below.

i) Landslides and liquefaction occurred respectively in volcanic mountainous and plain sites

ii) Both gentle and steep embankments of residential areas founded on volcanic ash cohesive soil deposits flowed and collapsed during a period of maximum

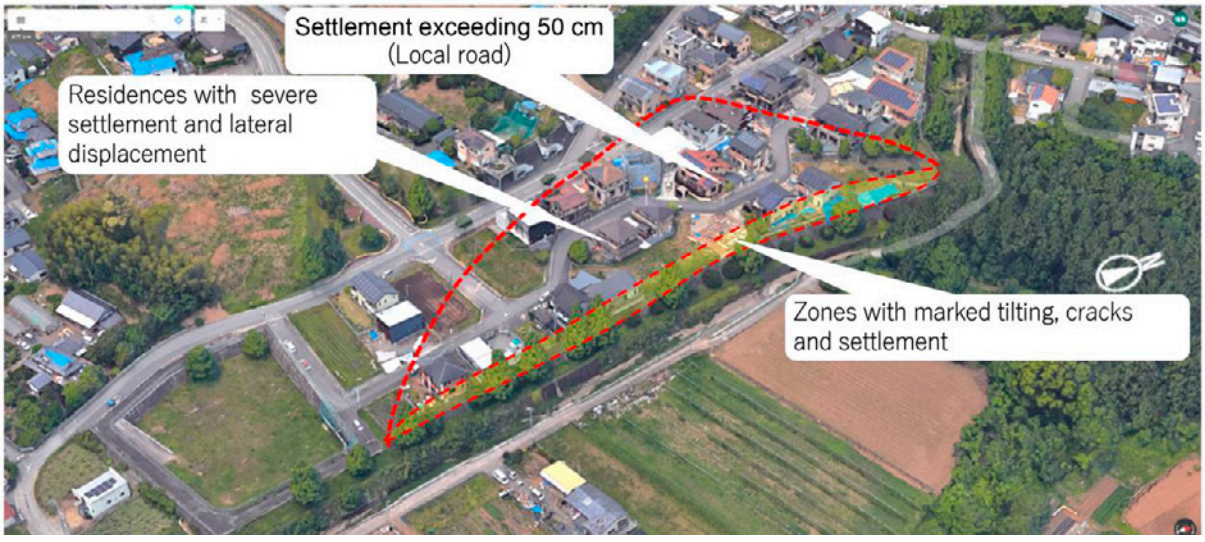


Photo 1 Example of damage features in residential areas.

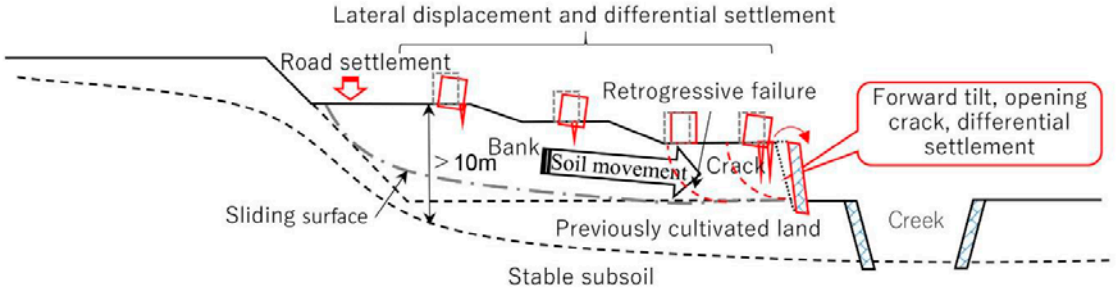


**Fig. 2.** Key sketch of the damaged embankment for residences.

seismic intensity, measured as 7. Particularly, residences with retaining walls were the most severely damaged.

iii) Volcanic ash soil is an important keyword associated with geo-disasters.

iv) Rich groundwater in Kumamoto plain played an important role in exacerbating damage to earth structures and foundations

One example of the damage features to residential areas is shown in Photo 1. A key sketch is presented in Figure 2. The authors inferred at least two reasons to explain how and why severe damage was induced by the earthquake, as described below.

(i) soil embankments used as residential foundations lost strength and stiffness, leading to collapse, severe settlement, and deformation

(ii) predominant nonlinearity and amplification of ground motion degraded the stiffness and strength of volcanic ash cohesive soils, leading to large lateral displacement

Based on the concept (ii) above, the inferred mechanism of damage to embankments and residences is presented in Fig. 3 which depicts the following:

i) Rocking motion of residences and retaining walls caused by the earthquake-induced degradation and decreased strength and stiffness of foundation soils of residences and backfill soils of retaining walls.

ii) Foundations lost bearing capacity; retaining walls were subjected to increased lateral earth pressures.

According to the mechanism explained above, we present a proposed a methodology for evaluating the instability of residences on embankments and subsoils with volcanic-origin cohesive soils, which in this case sustained two strong earthquakes (magnitude of 7) in a short time.

## 3. Characteristics of volcanic ash cohesive soils associated with increasing residential damage

### *3.1 Subsoil conditions at the site.*

The site investigation conducted by AIST after the Kumamoto earthquake revealed that the typical subsoil profile of Miyazono district in Mashiki town in Kumamoto, which was most severely damaged as is depicted in Fig. 3, It has deposits of soft volcanic ash cohesive soils covered by a loam layer and an embankment (Yoshimi et al., 2017).

### *3.2 Index properties of volcanic ash-cohesive soils.*

Figure 3 shows that AIST sampling was conducted at the location where residences were damaged most severely.

Before dynamic triaxial shear deformation tests at laboratory, index tests including Atterberg limit tests and grain size distribution tests were conducted on volcanic ash cohesive soils sampled from the site labeled as TMP3 in Figure. 3. Results obtained from both typical index tests are presented in Table 1. From them, the plasticity chart and the grain size distribution curves are depicted, respectively, in Figures 4 and 5. According to results from both index tests, soil specimens are classified as compressible silt-rich cohesive soils with low strength and high water content.

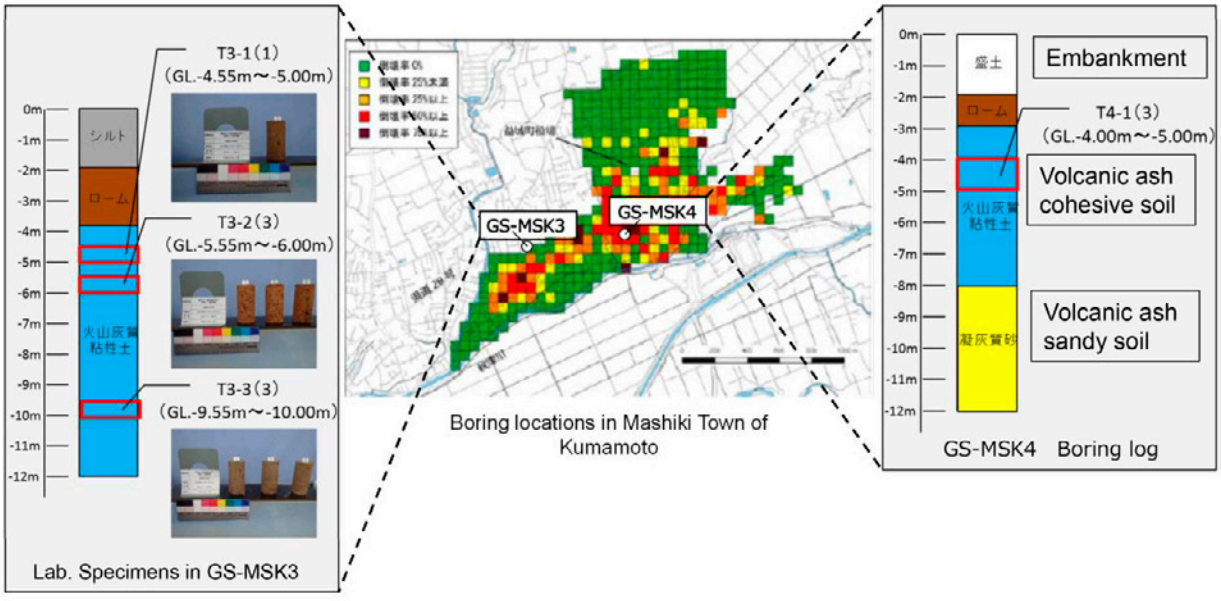


**Fig. 3.** Investigation site and borehole log at two locations.

**Table 1 Index properties of volcanic ash cohesive soils**

| Specimen number | GS-MSK-2 T2-1 | GS-MSK-2 T2-2 | GS-MSK-3 T3-1 | GS-MSK-3 T3-2 | GS-MSK-3 T3-3 |
|---|---|---|---|---|---|
| Depth (m) | 0.50--1.00 | 1.50--2.00 | 4.55--5.00 | 5.55--6.00 | 9.55--10.00 |
| Density of soil particle $\rho_s$ (t/m$^3$) | 2.487 | 2.646 | 2.763 | 2.771 | 2.756 |
| Initial void ratio $e_0$ | 3.06 | 2.098 | 2.15 | 2.094 | 1.728 |
| Initial water content $w_0$ (%) | 112.1 | 78.8 | 74.2 | 73.3 | 63.3 |
| Degree of saturation $S_r$ (%) | 91.1 | 99.4 | 95.3 | 96.9 | 100 |
| Liquid limit $w_L$ (%) | 131 | 106 | 72 | 69.6 | 63.4 |
| Plasticity index $I_p$ | 55.4 | 51.6 | 34.8 | 35 | 31.1 |
| Finer content $F_c$ (%) | 91 | 84 | 88 | 84 | 60 |
| Unified soil classification | MH-S | $VH_2$-S | $VH_1$-S | $VH_1$-S | MHS-G |
| Initial shear modulus $G_0$ (MN/m$^2$) | 8.27 | 9.34 | 27.47 | 27.47 | 35.34 |
| Effective confining pressure $\sigma'_c$ (kN/m$^2$) | 30 | 35 | 65 | 75 | 90 |
| Normalized initial shear modulus $G_0/\sigma'_c$ | 275.7 | 266.9 | 422.6 | 366.3 | 392.7 |
| Soil characteristics | Embankment (Artificial mixture of loam with silt) | | Tuffaceous silt | | |

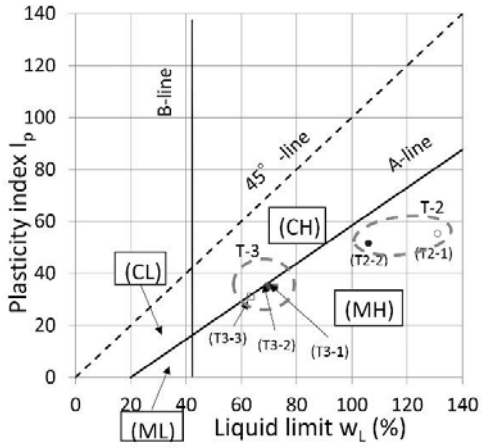


**Fig. 4.** Plasticity chart of volcanic cohesive soils.

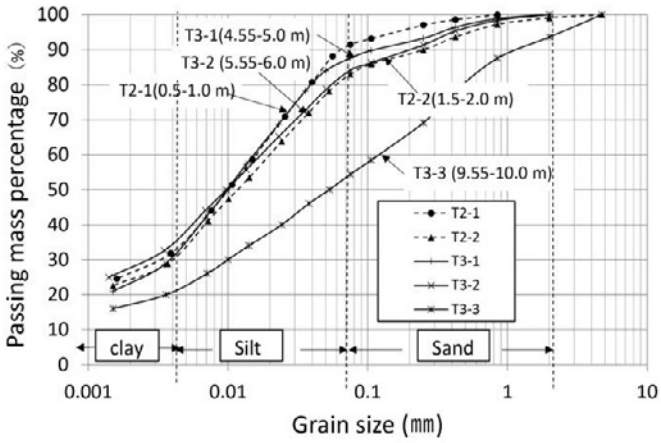


**Fig. 5.** Grain size distribution curves of volcanic cohesive soils.

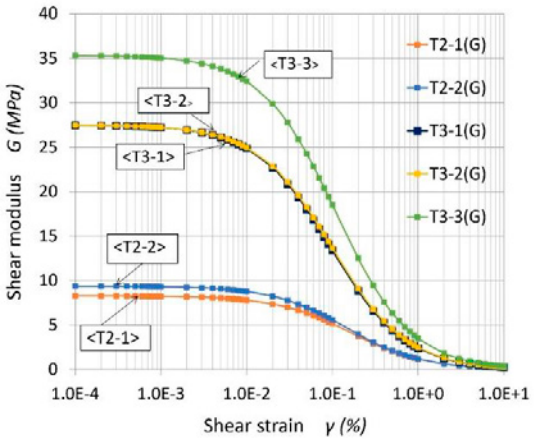


**(a) Shear modulus vs. shear strain relation**

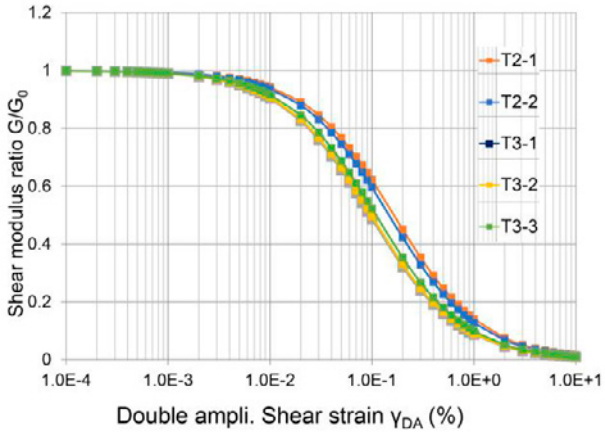


**(b) Shear modulus ratio vs. shear strain relations**

**Fig. 6.** Shear modulus and shear modulus ratio vs. shear strain relation.

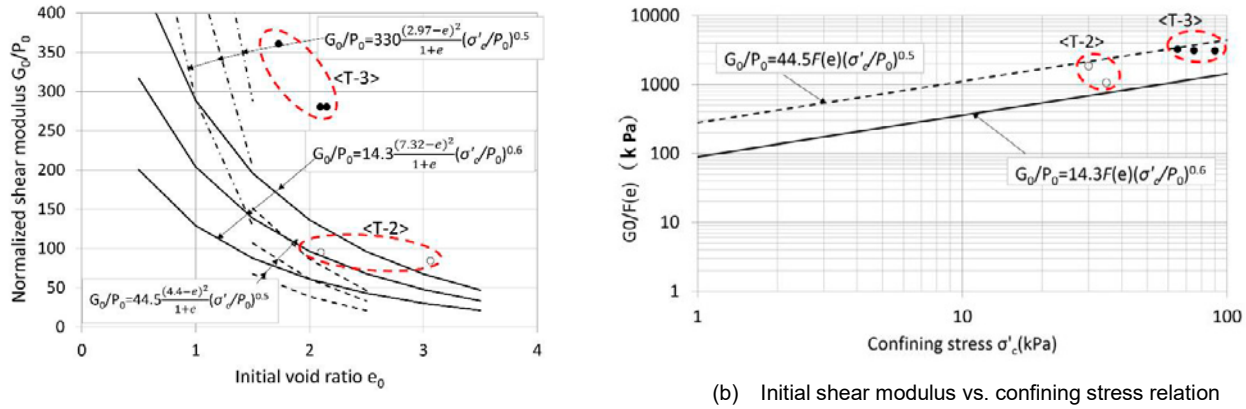


(a) Initial shear modulus vs. initial void ratio relation

(b) Initial shear modulus vs. confining stress relation

**Fig. 7.** Dependency of initial shear modulus on initial void ratio and confining stress.

Therefore, it was surmised that these volcanic-ash cohesive soils were related to severe residential damage in Mashiki Town during two great great earthquakes in Kumamoto.

Shear modulus and shear strain relations obtained from dynamic triaxial deformations tests are presented for five specimens in Figure 6. The initial shear moduli obtained by extrapolation of five curves shown in Figure 6 are shown in Figure 7 against the initial void ratio and the confining pressure which each specimen undergoes at the site. Thick curves in Figure 7 were calculated using empirical formulas proposed by Hardin and Black (1968), Marcuson and Wahls (1972), and Kokusho et al. (1982).

The authors suspect that this nonlinearity of ground response at Mashiki Town during the 2016 Kumamoto earthquake followed by ground motion amplification induced softening the volcanic ash cohesive soils, leading to severe damage to residences (Yoshimi et al., 2017; Yasuhara et al., 2017).

## 4. Prediction of earthquake-induced settlement and deformation

### *4.1 Method for predicting cyclic-induced settlement*

As shown in Figure 8, settlement induced by such cyclic loading as earthquakes induces settlement $\Delta S_{i,cy}$ immediately after an earthquake ($t$ = 0) and settlement $\Delta S_{vr}$ ($t$ > 0) followed by $\Delta S_{i,cy}$, which results from dissipation of excess pore water pressure generated during earthquakes.

$$\Delta S_{cy} = \Delta S_{icy} + \Delta S_{vr} \qquad [1]$$

By referring to Figure 9, both $\Delta S_{icy}$ is given as shown below.

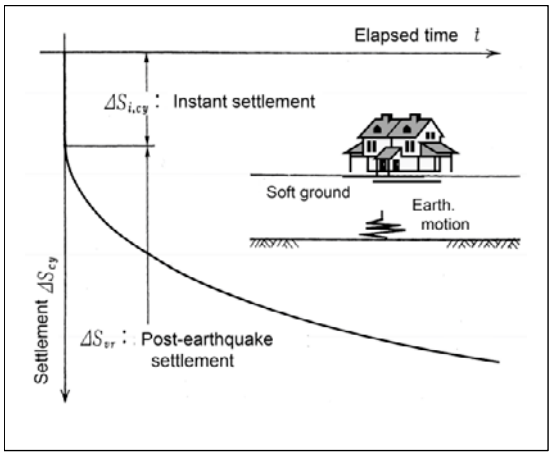


**Fig. 8.** Constitution of earthquake-induced settlements of structures on cohesive soils.

$$\Delta S_{icy} = S_{iNC}\left\{\frac{R_q}{R_k}\left(\frac{1-1/F_s}{R_q-1/F_s}\right)\right\} \qquad [2]$$

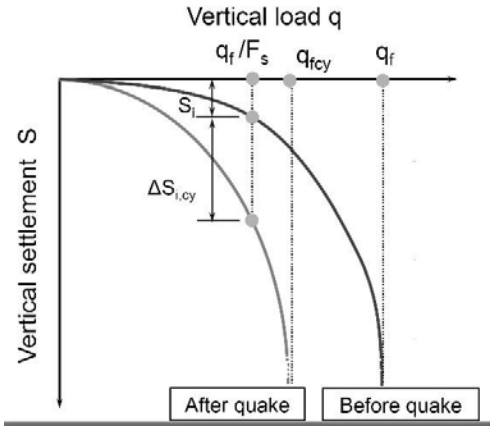


**Fig. 9.** Vertical load vs. settlement relations of residences before and after the earthquake.

where $S_{iNC}$ stands for instant settlement under a structural dead load by, $Fs$ is a safety factor of bearing

capacity, $R_q$ and $R_k$ are earthquake-induced degradation indices in strength and stiffness, expressed respectively as shown below.

$$\frac{s_{u,cy}}{s_{u,NC}} = n_q^{\Lambda_0/\Lambda-1} \qquad [3a]$$

$$\frac{E_{cy}}{E_{NC}} = \frac{1-C/\Lambda \ln(n_q)}{n_q} \qquad [3b]$$

Parameters $\Lambda_o$, $\Lambda$ and $C$ are defined as

$$\Lambda_0 = \frac{\log\{(s_u/p')_{OC}/(s_u/p')_{NC}\}}{\log OCR} \qquad [4]$$

$$\Lambda = 1 - C_s/C_c \qquad [6]$$

$$C = \frac{(E/p')_{OC}/(E/p')_{NC}}{\ln OCR}. \qquad [7]$$

Accordingly, $n_q$ can be given by:

$$n_q = 1/(1 - \Delta u_{cy}/\sigma'_c), \qquad [8]$$

in which $\Delta u_{cy}$ denotes the excess pore pressure generated during the earthquake. Additionally, $\sigma'_c$ is the confining pressure.

*4.2 Post-earthquake settlements caused by dissipation of excess pore pressures*

As shown in Figure 10, post-earthquake time-dependent settlement caused by dissipation of excess pore pressures can be given as

$$\Delta S_{vr} = H \frac{C_{rcy}}{1+e_0} \log(n_q) \qquad [9]$$

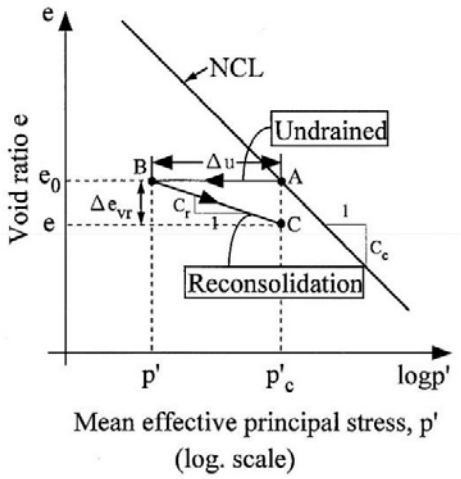


**Fig. 10.** *e* vs. log. *p'* relations of cohesive soils before and after earthquake loading.

where $C_{rcy}$ is the recompression index, and where $e_o$ is the initial void ration, as defined in Figure 10.

Combination of Eq. (1) with Eq. (2) and Eq. (9) yields the following expressions.

$$\Delta S_{cy} = \Delta S_{icy} + \Delta S_{vr} = S_{iNC}\left\{\frac{R_q}{R_k}\left(\frac{1-1/F_s}{R_q-1/F_s}\right)\right\} + H\frac{C_{rcy}}{1+e_0}\log(n_q) \qquad [10]$$

To calculate earthquake-induced settlement of residences constructed on cohesive volcanic ash soils using Eq. (10), one must merely determine such mechanical parameters as the pre-earthquake undrained strength and instant settlement of soil deposits and assume the pre-earthquake average weight of residence $\Delta q$ to calculate the residence settlement.

## 5. Simplified Method for Predicting Earthquake-induced Shear Deformation.

When we refer to Figure 11, the earthquake-induced shear strain is given as presented below.

$$\Delta\gamma = (1+\nu)\frac{\sigma_{vi}}{E_i}\left\{\left(\frac{E_{cyc}}{E_i}\right)^{-1} - 1\right\} \qquad [11]$$

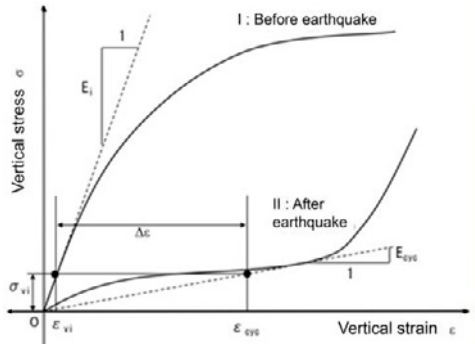


**Fig. 11.** Vertical stress vs. vertical strain relations of cohesive soils before and after earthquake (After Yasuda et al, 1999).

The idea is similar to the method for liquefaction-followed lateral deformation of sand. Substitution of Eq. (3b) into Eq. (11) yields the following.

$$\Delta\gamma = (1+\nu)\frac{\sigma_{vi}}{E_i}\left\{\left(\frac{n_q}{1-(C/\Lambda)\ln(n_q)}\right) - 1\right\} \qquad [12]$$

Therefore, we obtain the earthquake-induced incremental shear deformation expressed shown below.

$$\Delta\delta = H\Delta\gamma = H(1+\nu)\frac{\sigma_{vi}}{E_i}\left\{\left(\frac{n_q}{1-(C/\Lambda)\ln(n_q)}\right)-1\right\} \quad [13]$$

## 6. Instability of residences founded on volcanic ash cohesive soils

### *6.1 Instability mechanism*

As described earlier, the authors infered that damage to residences on volcanic ash cohesive soils resulted from earthquake-induced nonlinearity of ground motions leading to degradation of soil stiffness and strength. This point is illustrated schematically in Figure 12, which implies that rocking forces of retaining walls and residences followed by the earthquake-induced inertia force degraded the foundation and backfill soil stiffness and strength.

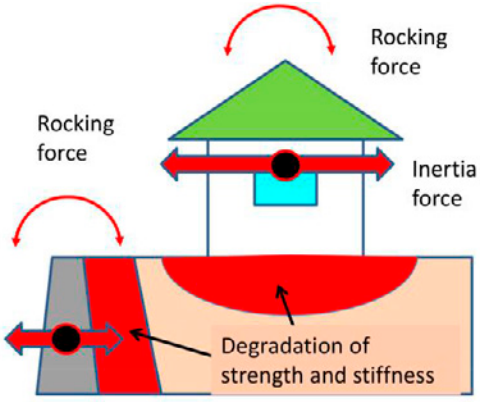


**Fig. 12.** Key sketch for cyclic degradation of foundations and backfill.

### *6.2 Foundation instability assessment*

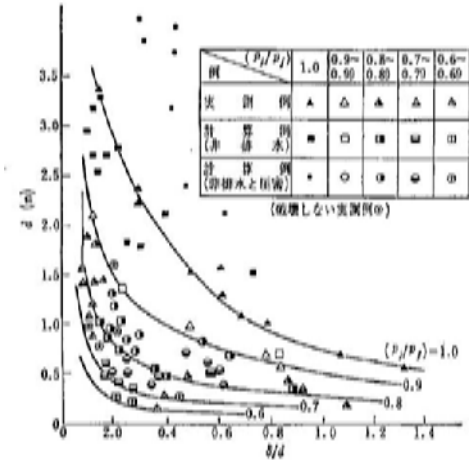

**Fig. 13.** Construction management diagram for embankment (Matsuo and Kawamura, 1978).

Instability of residences on volcanic ash cohesive soils was estimated as shown in Figure 13 as a diagram of embankment construction management in which $\Delta S_{icy}$ vs. $\Delta\delta/\Delta S_{icy}$ relations are presented as a parameter of the load ratio $p_i/p_f$ and safety factor $p_f/p_i$ which as Matsuo and Kawamura (1978) proposed.

Model ground for a set of calculations using the methodology presented in the previous section is shown in Figure 14. We should devote attention to the fact that no retaining wall is adjacent to the residence in this case.

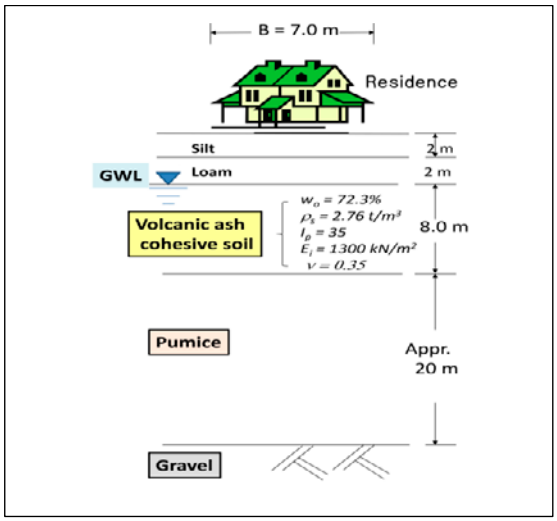


**Fig. 14** Model ground for instability assessment of residences

Behaviour of retaining walls will be mentioned in the following section.

### *6.3 Initial settlement by the dead load of the residence.*

First, the calculation of initial settlement $S_{i,NC}$ must be done for the 4.0 m deep volcanic ash soil layer with a dead load of a residence before the earthquake, given as

$$S_{i,NC} = I_\sigma \frac{1-\nu^2}{E_{NC}} qB \quad [14]$$

To start with calculation of settlement and deformation of volcanic ash cohesive soils, we assume the following.

i) The residence weight $q$ is equal to 20 kN/m$^2$;

ii) The Poisson ratio is fixed as 0.35, with Young's modulus for volcanic ash soil stiffness given as

$E_{NC} = 210\ s_{u,NC} = 210\ (s_u/p')\ p'_c = 1297.6$ kN/m$^2$

The influencing value $I_\sigma$ in Eq. (14) is determined as 0.71 for $B$ = 7 m and L = 12 m. Substituting these values into Eq. (14), we obtain

$S_{iNC} = 0.71 \times ((1-0.35^2)/1297.6)) \times 20 \times 7 = 6.7$ cm.

As described earlier, instant settlement immediately after the earthquake is evaluated using Eq. (2). Using the indices presented in Table 1, parameters included in Eq. (2) are given as shown below.

$\Lambda_0 = 0.635$, $\Lambda = 0.745$, $F_s = q_w/q = 5.14 \times 6.18/20 = 1.59$

Therefore, we obtain

$$R_q = n_q^{-0.148} \qquad [15]$$

and

$$R_k = \frac{E_{cy}}{E_{NC}} = \frac{1 - C/\Lambda \ln(n_q)}{n_q} = \frac{1 - 0.349 \times \ln(n_q)}{n_q} \qquad [16]$$

when $C$ is assumed as 0.26 (Wroth and Houlsby, 1978). Therefore, we obtain the following.

$$\Delta S_{icy} = S_{iNC}\left\{\frac{R_q}{R_k}\left(\frac{1 - 1/F_s}{R_q - 1/F_s}\right) - 1\right\}$$

$$= 6.7 \times \left\{\frac{n_q^{-0.148}}{\frac{1 - 0.349 \times \ln(n_q)}{n_q}}\left(\frac{1 - 1/F_s}{n_q^{-0.148} - 1/F_s}\right) - 1\right\} \qquad [17]$$

*6.4 Time-dependent settlement caused by excess pore pressure dissipation*

Settlement is calculable using Eq. (9). Here, using the indices given in Table 1, we have the following.

$e_o = w_o(\rho_s/\rho_w)/S_r = 2.05$ and $C_c = 0.602$

Consequently, time-dependent settlement caused by dissipation of excess pore pressure was estimated.

$$\Delta S_{vr} = H\frac{C_r}{1 + e_0}\log(n_q) = 800 \times \frac{0.225 \times 0.602}{1 + 2.050}\log(n_q)$$

$$= 33.5 \times \log(n_q) \qquad [17]$$

*6.5 Evaluation of instant lateral deformation.*

Using Eq. (13), instant lateral displacement was evaluated as shown below.

$$\Delta\delta = H\Delta\gamma = H(1+\nu)\frac{\sigma_{vi}}{E_i}\left\{\left(\frac{n_q}{1 - (C/\Lambda)\ln(n_q)}\right) - 1\right\}$$

$$= 0.128 \times \left\{\left[\frac{n_q}{1 - 0.282 \times \ln(n_q)}\right] - 1\right\} \qquad [19]$$

*6.6 Construction management diagram using settlement and deformation*

In the Matsuo and Kawamura (1978)'s construction management chart using $\Delta S_{iNC}$ vs. $\Delta\delta/\Delta S_{iNC}$ relations, a family of curves was shown in Figure 13, corresponding to safety factor $F_s$ (= $q_f/q_i$) equal to 1.0, 1.11, 1.25, 1.48, and 1.67.

Earthquake-induced settlement and deformation used for construction of this chart were calculated respectively using the first terms of Eq. (1) and Eq. (10) as a parameter of the normalized excess pore pressure expressed by $\Delta u_{cy}/\sigma'_c$. Then, the diagram of $\Delta S_{icy}$ vs. $\Delta\delta/\Delta S_{icy}$ relations is constructed following the procedure proposed by Matsuo and Kawamura (1978). Here, $\Delta S_{cy}$ vs. $\Delta\delta/\Delta S_{cy}$ relations are presented in the same type of figure for comparison. In this case, the effect of time-dependent settlement caused by dissipation of excess pore pressures is also reflected in the diagram for instability of residences on cohesive soils. This aspect is slightly different from the original chart proposed by Matsuo and Kawamura.

Calculated results of earthquake-induced settlement and lateral deformation using Eqs. (16) - (18) are shown against excess pore water pressure $\Delta u_{cy}$, normalized by the vertical effective stress $\sigma'_{vi}$, as shown in Figure 15. Earthquake-induced settlement vs. $\Delta u_{cy}/\sigma'_{vi}$ relations are divisible into cases of $\Delta S_{icy}$ vs. $\Delta u_{cy}/\sigma'_{vi}$ and $\Delta S_{vr}$ vs. $\Delta u_{cy}/\sigma'_{vi}$. Apparently, an inflection point of the curves exists between 0.7 and 0.8 of the normalized excess pore water pressure, $\Delta u_{cy}/\sigma'_{vi}$.

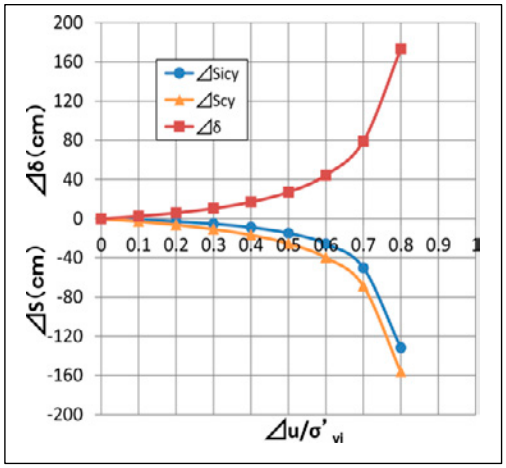


**Fig. 15.** Settlement and deformation vs. normalized excess pore water pressures relations.

The calculated results of settlement $\Delta S_{icy}$ and $\Delta S_{cy}$ and lateral deformation $\Delta\delta$ are combined as a design chart in which $\Delta S_{icy}$ and $\Delta S_{cy}$ are shown respectively against $\Delta\delta/\Delta S_{icy}$ and $\Delta\delta/\Delta S_{cy}$ in Figure 16 along with theoretical

curves proposed by Matsuo and Kawamura (1978), which were constructed in terms of the observed data at the actually constructed embankment. Comparison of the results reveals their mutually differing tendencies: $\Delta\delta/\Delta S_{icy}$ and $\Delta\delta/\Delta S_{cy}$ approach the failure line with $q_f/q$ = 1.0 by decreasing or increasing, whereas $\Delta S_{icy}$ and $\Delta S_{cy}$ increase in both cases. Figure 16 also suggests that the excess pore water pressure ratios in both cases corresponding to the intersection point of the theoretical curve with the observed plot exist at about 0.70, which agrees well with the tendency presented in Figure 15.

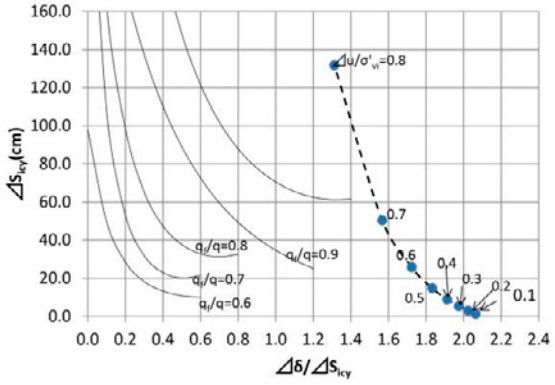


(a) Without volumetric settlement considered

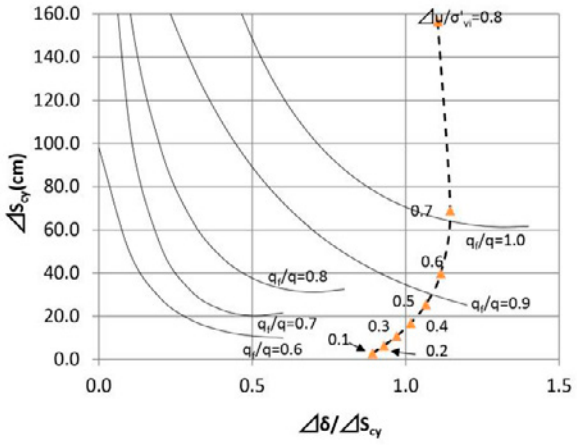


(b) With volumetric settlement considered

**Fig. 16.** Plots of calculated results on the chart of construction management.

## 7. Earthquake-induced bearing capacity decrease and retaining wall degradation

As well as additional settlement and deformation of foundations, the great earthquakes in Kumamoto in 2016 must induce instability of structures on residences and adjacent wall structures.

### *7.1 Decrease in bearing capacity in the residential foundation*

Let us first consider how severe the earthquakes give influences on the residences in Mashiki Town.

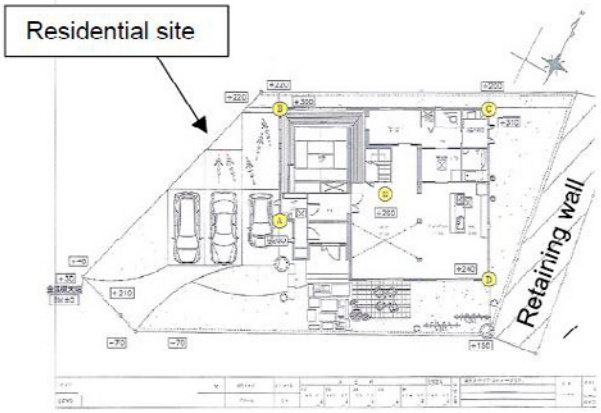


**Fig. 17.** Locations in the residence with SWS measurement before and after earthquakes

There exists an evidence which supports the decrease in bearing capacity of foundation ground of a residential site before and after the earthquakes, as is shown in Figure 17, where the Swedish Weight Sounding (SWS) tests were conducted by the house maker. The results of SWS tests before and after earthquakes are plotted against depth at 5 locations in Figure 18. Comparison of the results obtained between before and after the earthquakes showed SWS results indicating that bearing capacity, $q_a$, equal to 28..6 kN/m$^2$ after the earthquakes became 35.5 kN/m$^2$ before the earthquakes. Those calculation was carried out by using

$$q_a = 30\,\overline{W_{sw}} + 0.64\,\overline{N_{sw}} \qquad [20]$$

which is proposed by Architectural Institution of Japan (2014).

Therefore, bearing capacity decreased approximately 20% because of the earthquake motion. Because this must have influenced on earth pressures acting against the retaining walls, we can examine the influence of bearing capacity decrease of earth pressures on retaining walls. We assume that decreased bearing capacity of volcanic ash cohesive soils is equivalent to the loss of undrained strength, which must influence the change of earth pressures acting against retaining walls.

### *7.2 Degradation of retaining walls adjacent the residences*

As was described earlier in this paper, a number of retaining walls for embankment were severely damaged, triggering the devastating collapse of residences.

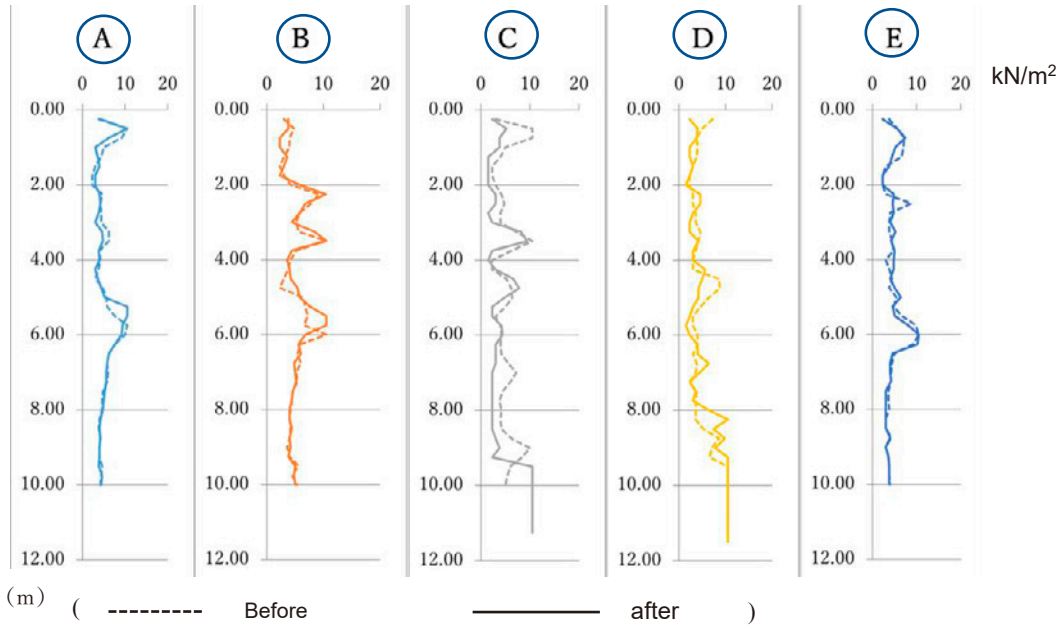


**Fig. 18.** Results of SWS at 5 locations in the residence before and after the earthquakes

Although earth pressure against retaining walls during earthquakes is normally evaluated using the seismic intensity method or the modified seismic intensity method, the authors understand that the rocking action caused by the large inertial force degraded the strength and stiffness of volcanic ash cohesive soils used as backfill materials for retaining walls close to residences. Moreover, they suspect that strength reduction damages the retaining wall, as shown in Figure 2.

Active and passive earth pressures acting against the retaining wall adjacent to the residence are presented in Figure 19. They are given as shown below.

$$P_A = \frac{1}{2}\gamma_t H^2 K_A - 2cH\sqrt{K_A} \qquad [20a]$$

$$P_P = \frac{1}{2}\gamma_t H^2 K_P + 2cH\sqrt{K_P} \qquad [20b]$$

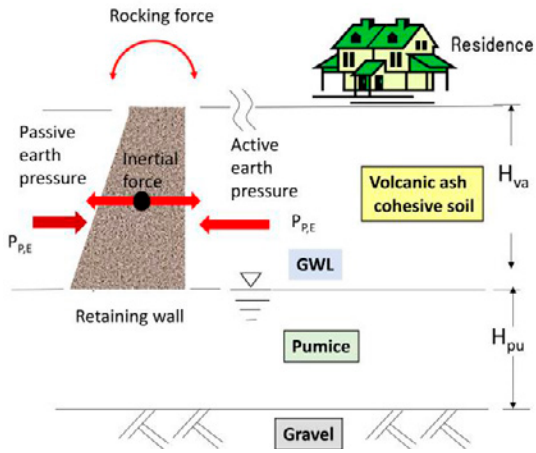


**Fig. 19.** Seismic earth pressures acting against retaining walls close to residence at earthquake

$K_A$ and $K_P$ In Eqs. (20a) and (20b) are the coefficients of active and passive earth pressures which are a function of the internal frictional angle, $\phi$.

In cases of zero internal frictional angle for volcanic ash cohesive soils, we have

$$P_A = \frac{1}{2}\gamma_t H^2 - 2s_u H \qquad [21a]$$

$$P_P = \frac{1}{2}\gamma_t H^2 + 2s_u H \qquad [21b]$$

where $s_u$ represents undrained strength of volcanic ash soils. If this undrained strength $s_u$ is assumed to decrease to $s_{u,cy}$ after the earthquake, then we have the following equations.

$$P_{AE} = \frac{1}{2}\gamma_t H^2 - 2s_{u,cy} H \qquad [22a]$$

$$P_{PE} = \frac{1}{2}\gamma_t H^2 + 2s_{u,cy} H \qquad [22b]$$

where $s_{u,cy}$ is post-earthquake undrained strength of volcanic ash soils. The question is how undrained strength, $s_u$, of the volcanic ash cohesive soils was degraded by the seismic motion to $s_{u,cy}$. Here, using the fact that measured bearing capacity after the earthquakes decreased by 20%, then in terms of back calculation using the equation

$$q_a = 5.14 s_u \qquad [23]$$

we obtain the respective undrained strengths before and after the earthquakes as 6.91 kN/m$^2$ and 5.56 kN/m$^2$, respectively. Using these values of undrained strength, we obtained the respective seismic earth pressures 79.3 kN/m for $P_{A,E}$ and 168.2 kN/m for $P_{P,E}$ against the retaining wall with 5.0 m high with index properties of backfill soils as shown in Fig. 21. Those are 26% for the active earth pressure smaller and 6% for the passive earth pressure larger than earth pressures without experience of the earthquakes. Therefore, those must contribute to the collapse of retaining walls under the earthquake, although they contributed to the increased instability of the retaining walls. However, further investigation should be conducted to clarify this point, particularly by adopting the Coulomb theory of earth pressures on retaining walls to which cannot be referred in the present paper.

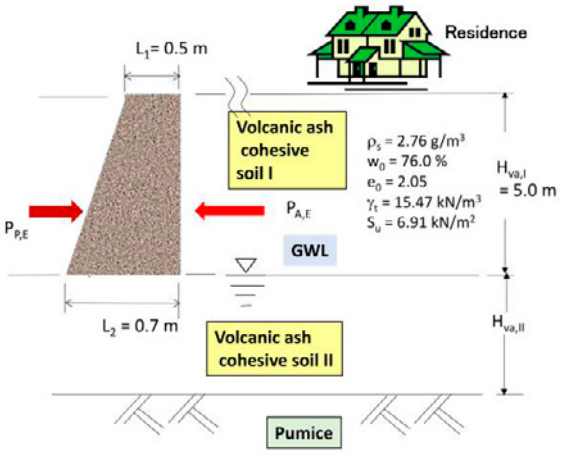


**Fig. 20.** An example of seismic earth pressures against retaining walls

## 8. Conclusion

This paper has presented a simplified methodology for evaluating the instability of residences constructed on volcanic ash cohesive soils during a large-scale earthquake as in the case of the 2016 Kumamoto earthquake. The method evaluates settlement and lateral deformation caused by cyclic degradation of strength and stiffness induced by nonlinear ground motion during an earthquake. The calculated results were used to evaluate the instability of residences during the Kumamoto earthquake in 2016. A chart for construction management of embankment and residences incorporating the results in terms of settlement vs. lateral deformation and settlement relations suggests that residences are likely to sustain severe damage when the normalized excess pore pressures generated during the earthquake exceed around 0.7 - 0.8.

The latter part of the paper presents an additional attempt to estimate the influence of cyclic degradation in strength and stiffness of volcanic cohesive soils on increase in lateral earth pressures against retaining walls adjacent to the residences. Conclusively, increased lateral earth pressures were estimated as approximately 20%. However, it remains uncertain whether this increase was a main factor causing the collapse of retaining walls during the great earthquakes.

## Acknowledgment

Research for this paper was supported financially by a Grant-in-Aid (No.16H02362) from the Ministry of Education, Culture, Sports, Science and Technology (MEXT) to representative Kazuya Yasuhara, Professor Emeritus of Ibaraki University, Japan. The authors express their sincere gratitude for this support.

## References

Architechtural Institute of Japan, 2014. Recommendation for Design of Small Building Foundations, 7th edition, pp. 74-75, (in Japanese).

Hardin, B. O. and Black, W. L., 1968. Vibration modulus of normally consolidated clay, *Proc. SMFD, ASCE*, **94**(2), 353-369.

Kokusho, T. Esashi, Y. and Yoshida,Y., 1982. Dynamic properties of soft clay with wide strain range, *Soils & Foundations,* **13**(1), J. JGS: 1-18.

Kusakabe, O. and Kawai, N., 1989. Reduction in bearing capacity and increase in settlement of a footing due to an upward seepage flow, *J. Japan Geotechnical Society,* **37**(6): 57-62, (in Japanese).

Marcuson, W. F. and Wahls, H. E., 1972. Time effects on dynamic shear modulus of clays, *Proc. SMFD, ASCE*, **98**(12): 1359-1373.

Matsuo, M. and Kawamura, K., 1978. Diagram for construction control of embankment on soft ground, *J. of JGS (Tsuchi-to-Kiso)*, 26(7): 245, 1-6, (in Japanese).

Tajiri, S., 2017. Damaged situation of residential area of Mashiki-town, *Proceedings of the International Workshop on the 2016 Kumamoto Earthquake,* pp. 75-84, March 6, 2017, Fukuoka, Japan.

Wroth, C. P. and Houlsby, G. T., 1985. Soil mechanics – Property characterisation and analysis procedures, *Proc. 11th ICSMFE*, 1, 1–56.

Yasuda, S., Yoshida, N., Adachi, K., Kiku, H., Gose, S. and Masuda, T., 1999. A simplified practical method for evaluating liquefaction-induced flow, J. of JSCE, No. 638/III-49, 71-89 (in Japanese).

Yasuhara, K., Murakami, S. Toyota, N., and Hyde, A. F. L., 2001. Settlements in fine-grained soils under cyclic loading, *Soils and Foundations*, **41**(6): 25–36.

Yasuhara, K., Hyde, A. F. L. and Murakami, S., 2004. Post-cyclic degradation of saturated plastic silts, *Proc. International Symp. on Cyclic Behaviour of Soils and Liquefaction Phenomena*, Bochum, Germany, 275–286.

Yasuhara, K. and Kazama, M., 2015. Land subsidence of clay deposits after the Tohoku-Pacific Ocean Earthquake, Proc. IAHS, 372, 211-216, Nagoya, Japan.

Yasuhara, K., Kobayashi, K., Watanabe, H., Yoshimi, M., Arai, Y., Hosoya, T. and Murakami, S., 2017. Instability of residences on volcanic ash cohesive soils during the 2016 Kumamoto Earthquake, *Proceedings of the International Workshop on the 2016 Kumamoto Earthquake March 6, 2017, Fukuoka, Japan*

Yoshimi, M., Goto, H., Hata, Y., and Yoshida, N., 2017. Nonlinear site response at the worst-hit area of the 2016 Kumamoto earthquakes in the Mashiki Town, Kumamoto, Japan, *DPRI Kyoto University Annual Meeting 2017*, A05.

**Symbols and abbreviations**

| | |
|---|---|
| B | Width of structure |
| C | Stiffness degradation parameter |
| $C_c$, $C_r$ | Compression and recompression indices |
| $C_{c,cy}$, $C_{r,cy}$ | Compression and recompression indices |
| $e_o$ | Initial void ratio |
| E, $E_{cy}$ | Deformation modulus before and after earthquake |
| $F_s$ | Safety factor of bearing capacity |
| G | Shear modulus |
| H | Height of cohesive soil layer |
| $I_\sigma$ | Settlement influencing value |
| $n_q$ | Earthquake-induced pore pressure index |
| p, P | Lateral earth pressures |
| q | Load by embankment |
| $R_q$, $R_k$ | Strength and stiffness degradation index |
| $S_{cy}$ | Earthquake-induced settlement |
| $S_i$, $S_{i,cy}$ | Instant settlement before and after earthquake |
| $S_{vr}$, $S_{vr,cy}$ | Recompression settlement before and after earthquake |
| $s_u$, $s_{u,cy}$ | Undrained strength before and after earthquake |
| $u_{cy}$ | Excess pore pressure generated by earthquake |
| $\gamma_t$ | Unit volume weight of soil |
| $\gamma_{cy}$ | Earthquake-induced shear strain |
| $\delta_{cy}$ | Earthquake-induced lateral deformation |
| $\Lambda$ | Irreversible index (= 1- $C_r/C_c$) |
| $\Lambda_o$ | Strength degradation parameter |
| $\rho_s$ | Density of soil particles |
| $\sigma'_{vi}$ | Effective overburden stress |